

Detector-Agnostic Phase-Space Distributions

J. Sperling,^{1,*} D. S. Phillips,² J. F. F. Bulmer,² G. S. Thekkadath,² A. Eckstein,² T. A. W. Wolterink,²
J. Lugani,² S. W. Nam,³ A. Lita,³ T. Gerrits,³ W. Vogel,⁴ G. S. Agarwal,⁵ C. Silberhorn,¹ and I. A. Walmsley²

¹*Integrated Quantum Optics Group, Applied Physics, University of Paderborn, 33098 Paderborn, Germany*

²*Clarendon Laboratory, University of Oxford, Parks Road, Oxford OX1 3PU, United Kingdom*

³*National Institute of Standards and Technology, 325 Broadway, Boulder, CO 80305, USA*

⁴*Institut für Physik, Universität Rostock, Albert-Einstein-Straße 23, D-18059 Rostock, Germany*

⁵*Texas A&M University, College Station, Texas 77845, USA*

(Dated: April 25, 2019)

The representation of quantum states via phase-space functions constitutes an intuitive technique to characterize light. However, the reconstruction of such distributions is challenging as it demands specific types of detectors and detailed models thereof to account for their particular properties and imperfections. To overcome these obstacles, we derive and implement a measurement scheme that enables a reconstruction of phase-space distributions whose functionality does not depend on the knowledge of the detectors, thus defining the notion of detector-agnostic phase-space distributions. Our theory presents a generalization of well-known phase-space quasiprobability distributions, such as the Wigner function. We implement our measurement protocol, using transition-edge sensors without performing a detector characterization. Based on our approach, we reveal the characteristic features of heralded single- and two-photon states in phase space and certify their nonclassicality with high statistical significance.

I. INTRODUCTION

The characterization of quantum light is a main challenge one encounters when implementing classically infeasible tasks, such as quantum communication protocols [1–3]. On a more fundamental level, studying the peculiarities of quantized radiation fields leads to a profound understanding of the role of quantum physics in nature in general, and how it is distinct from classical wave theories in particular. As in classical systems, quantum-optical phase-space distributions offer a versatile instrument to directly visualize unique features of nonclassical light, such as demonstrated for squeezing [4–6]. Moreover, negativities in certain phase-space functions directly point at quantum properties of light; see, e.g., Refs. [7–12]. For the above reasons, the representation of quantum light in phase space is one of the most frequently applied methods to characterize nonclassical light.

However, the estimation of phase-space distributions from experimental data is a cumbersome task. Consequently, this reconstruction problem inspired a wide range of research [13–15], leading to sophisticated analytical tools, such as solving inversion problems [16, 17], employing diverging pattern functions [18, 19], performing maximum-likelihood estimations [20, 21], and using data pattern recognition [22, 23]. In addition, each family of detection devices has to be equipped with its own precise model to reliably extract information about phase-space functions [13–15]. This treatment comprises a comprehensive analysis that assesses (i) how a detector responds to incident light [24, 25], including, e.g., nonlinear detection responses [26, 27], and (ii) how the light absorption is influenced by a number of possible imperfections, e.g., efficiencies [28, 29]. Moreover, applying these methods can also require universally applicable, yet rather demanding

theoretical and experimental techniques in practice, such as performing detector tomography and calibration [30–38].

Despite these challenges, phase-space distributions constitute a highly successful approach to revealing nonclassical properties of light [7–12]. For example, s -parametrized quasiprobabilities [39, 40], as well as their non-Gaussian generalizations [41, 42], can exhibit negativities which are incompatible with classical light. Even if a phase-space function does not exhibit negativities, observable patterns render it possible to identify quantum features, for instance, via the non-negative Husimi function [43–45] or through marginal distributions [46, 47]. Because of its success, the concept of phase-space functions has been further extended to other physical scenarios; see Ref. [48] for a thorough list. To name a few, atomic ensembles [49–52] and entanglement [53–55] have been successfully characterized using quasiprobability distributions. Nevertheless, there remains a dependency on well-defined detection schemes and reconstruction algorithms.

In this contribution, we circumvent the reconstruction problem by devising a measurement protocol that results in detector-agnostic phase-space (DAPS) distributions, which can be directly estimated and encompass known quasiprobabilities. We demonstrate our scheme with transition-edge sensors (TESs), which have sophisticated physics underlying their operation, and we analyze our data without relying on any specific detector models. Our DAPS functions reveal nonclassical features expected from our generated heralded multiphoton states with high statistical significance. Moreover, the measurement of vacuum alone enables us to predict the unique structures of DAPS distributions as demonstrated for our experimentally generated states.

II. THEORY FRAMEWORK

Our measurement scheme is a combination of unbalanced homodyning [56] and a multiplexed detection layout [57]; see

* jan.sperling@uni-paderborn.de

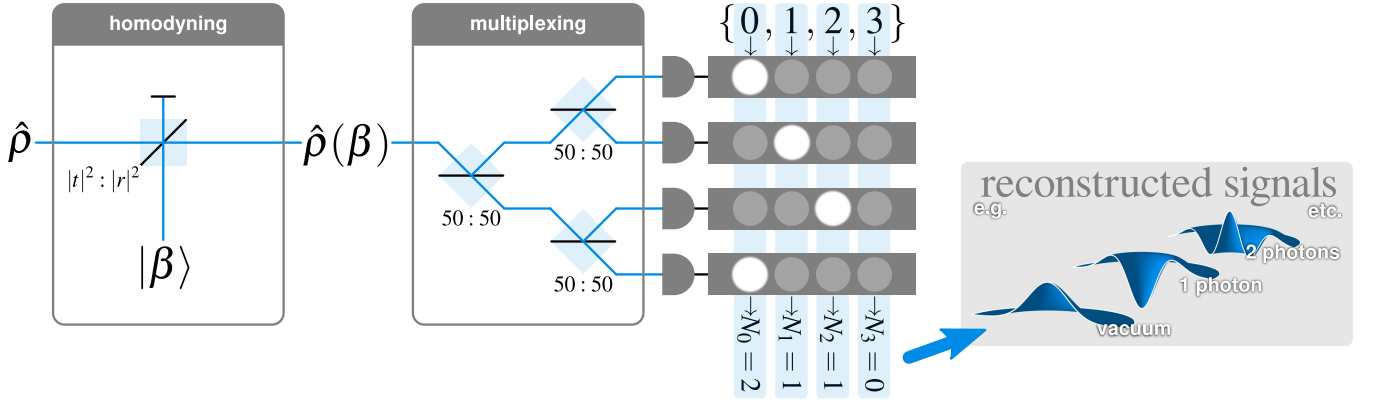


FIG. 1. Protocol overview. A signal state $\hat{\rho}$ is mixed on a $|t|^2 : |r|^2$ beam splitter with a LO $|\beta\rangle$ in an unbalanced homodyning configuration. The resulting state $\hat{\rho}(\beta)$ is fed into a multiplexing scheme (shown for $S = 2$ steps). Each output beam is measured with a detector that can produce some outcomes (here, $\mathcal{K} = \{0, \dots, K = 3\}$). The resulting statistics $c_{N_0, \dots, N_K}(\beta)$ is obtained, where N_k counts the number of outcomes k and $N_0 + \dots + N_K = N$. From the measured data, we directly estimate our generalized phase-space distributions, cf. the first line in Eq. (2).

Fig. 1. A signal light field, $\hat{\rho}$, is mixed with a local oscillator (LO), $|\beta\rangle$, on a beam splitter. One of the output states, represented through $\hat{\rho}(\beta)$, is injected into a multiplexing scheme which consists of S steps. In each step, light is split into output fields with the same intensity, which then can be split again. The finally obtained $N = 2^S$ output beams are individually measured with unknown detectors, which are not specified but assumed to operate in the same manner. Each detector returns one of the possible outcomes $\mathcal{K} = \{0, \dots, K\}$. In Refs. [58, 59], we have shown for the multiplexing part that independently of the detector response, the probability to simultaneously measure N_k times the outcome k ($\forall k \in \mathcal{K}$) follows a quantum version of multinomial distribution; its generalization to $\hat{\rho}(\beta)$ reads

$$c_{N_0, \dots, N_K}(\beta) = \left\langle : \frac{N!}{N_0! \dots N_K!} \hat{\pi}_0^{N_0} \dots \hat{\pi}_K^{N_K} : \right\rangle_{\hat{\rho}(\beta)}, \quad (1)$$

where $: \dots :$ denotes the normal ordering and $\{\hat{\pi}_k\}_{k \in \mathcal{K}}$ is the unknown positive operator-valued measure of the detectors.

The only assumptions made are a balanced splitting in the multiplexing and identical response functions for the N detectors, including all imperfections. We can account for deviations from both assumptions by including a systematic error, directly estimated from asymmetries in the measured data; see the Supplemental Material (SM) for details [60].

A probability distribution is entirely characterized through its generation function, which can be expressed as

$$\begin{aligned} g_{z_0, \dots, z_K}(\beta) &= \sum_{N_0, \dots, N_K} z_0^{N_0} \dots z_K^{N_K} c_{N_0, \dots, N_K}(\beta) \\ &= \left\langle : (z_0 \hat{\pi}_0 + \dots + z_K \hat{\pi}_K)^N : \right\rangle_{\hat{\rho}(\beta)}, \end{aligned} \quad (2)$$

for $z_0, \dots, z_K \in \mathbb{R}$. The second line is a result of the multinomial form of the statistics in Eq. (1). One salient feature is that classical light fields have a nonnegative generation function g_{z_0, \dots, z_K} . To see this, first recall that a classical light field is described through a nonnegative Glauber-

Sudarshan distribution [61, 62], which is not affected by displacements and describes a state as a statistical mixture of coherent states. Furthermore, for all even N , we can define the operator $\hat{f} = \hat{f}^\dagger = (z_0 \hat{\pi}_0 + \dots + z_K \hat{\pi}_K)^{N/2}$. As for any non-negative Glauber-Sudarshan function $\langle : \hat{f}^\dagger \hat{f} : \rangle \geq 0$ holds true [63–66], we conclude

$$g_{z_0, \dots, z_K}(\beta) \stackrel{\text{cl.}}{\geq} 0. \quad (3)$$

A violation of this inequality certifies the nonclassicality of the signal light, $\hat{\rho}$. We can also define a special case of this generating function,

$$G_z(\beta) = g_{1, z, z^2, \dots, z^K}(\beta). \quad (4)$$

Similarly to the expression in Eq. (2), G_z is straightforwardly estimated from the measured detector outcomes $c_{N_0, \dots, N_K}(\beta)$ by setting $z_k = z^k$, and G_z is nonnegative for classical light.

As an example, we may consider photocounting [24]. Although this model is not required for our approach and does not apply to our experiment (TESs have a finite photon-number resolution, a non-unit detection efficiency, and a non-linear response function [59]), it demonstrates how G_z generalizes the concept of well-known phase-space distributions. For photocounting, we find [60, 67]

$$G_z(\beta) = \langle : e^{-[1-z]\eta \hat{n}} : \rangle_{\hat{\rho}(\beta)} = \frac{\pi(1-s)}{2} P\left(\frac{r}{t} \beta; s\right), \quad (5)$$

with η and \hat{n} being the efficiency and the photon-number operator, respectively, and $s = 1 - 2/[\eta|t|^2(1-z)]$ [68]. Thus, $G_z(\beta)$ resembles the s -parametrized distributions $P(r\beta/t; s)$ [39, 40]. Beyond photoelectric detectors, we refer to g_{z_0, \dots, z_K} and G_z as DAPS distributions as Eqs. (2) and (4) apply without any knowledge of the measurement operators $\{\hat{\pi}_k\}_{k \in \mathcal{K}}$. In this context, it is worth emphasizing that the first line in Eq. (2) enables the estimation of our DAPS distributions as a result of the measured coincidence statistics $c_{N_0, \dots, N_K}(\beta)$ alone.

III. IMPLEMENTATION

By implementing a single multiplexing step, $N = 2$, we demonstrate how to apply our theoretical framework of DAPS distributions. To realize our protocol in Fig. 1, we produce heralded photon states $\hat{\rho}$ and different LO amplitudes β . The detectors used for the measurement and the heralding are TESs, which count photons up to a maximal number K . In the following, we briefly describe the experimental setup; see the SM [60] for more details.

Femtosecond pulses from a titanium sapphire laser are coupled into two separate, periodically poled potassium titanyl phosphate (ppKTP) waveguides. With the first ppKTP waveguide, we prepare the signal $\hat{\rho}$. Pumping the waveguide produces two-mode squeezed vacuum via type-II parametric down conversion (PDC) [69]. One mode is sent to a TES detector to herald photon states in the other mode. With the second ppKTP waveguide, we prepare the LO. In contrast to the signal state generation, we stimulate the PDC process by seeding it with pulses from a carved continuous-wave laser. Since the process is driven parametrically, wave mixing generates coherent light in the polarisation mode orthogonal to the seed [70]. The generated LO is attenuated to the single-photon level. Crucially, this process prepares a LO with Poissonian photon statistics and a spectrum that is well matched to the signal. Finally, the LO $|\beta\rangle$ and signal $\hat{\rho}$ are combined on a 90 : 10 beam splitter. We consider the port which uses $|r|^2 = 10\%$ of the LO and transmits $|t|^2 = 90\%$ of the signal. The light from this port, $\hat{\rho}(\beta)$, is then impinged on a 50 : 50 beam splitter for realizing a multiplexing step; both outputs are then sent to two separate TESs.

Our experiment uses three TES detectors [71], which can have efficiencies above $\eta = 90\%$ [72]. The TESs are superconducting devices operating in a dilution refrigerator with an operating temperature around 80mK. Their electrical response is amplified using an array of superconducting quantum interference devices [73], followed by further amplification and filtering at room temperature. This electrical signal is read by an analogue-to-digital converter and processed using a matched filter technique [74], which outputs a single value. We bin these values to determine the photon number. We note that although this technique is convenient, alternative binnings [59] can be used without affecting the applicability of the DAPS distribution approach.

We record the binned outcome at all three TESs for various LO amplitudes ($|\beta|^2$ from 0 to ~ 28 in steps of ~ 1). The amplitude is controlled by varying the seed laser power. To obtain data for a specific heralded state $\hat{\rho}$, we consider the subset of trials with the appropriate detection outcome (i.e., heralding bin k_h) at the herald TES.

IV. VERIFICATION OF NONCLASSICALITY

In a first step, we apply our DAPS distribution to uncover nonclassical features of our prepared states through the violation of condition (3). The optimal negativity we obtain from

TABLE I. For different heralding outcomes, k_h , we show the non-classicality criteria $\mu_{\min} < 0$ and $g_{\min} < 0$. g_{\min} is defined in Eq. (6). μ_{\min} is the minimal eigenvalue to the second-order correlation matrix M defined in Eq. (6) of Ref. [58]; see also the SM [60]. “−0” indicates a slightly negative mean value which rounds to zero.

k_h	μ_{\min}	g_{\min}
0	$(-0 \pm 9) \times 10^{-4}$	$(-0 \pm 2) \times 10^{-9}$
1	-0.15 ± 0.03	-0.026 ± 0.003
2	-0.10 ± 0.03	-0.017 ± 0.003

the DAPS function [Eq. (2)] is given by the minimum

$$g_{\min} = \min_{\beta} \min_{\substack{z_0, \dots, z_K \\ |z_0|^2 + \dots + |z_K|^2 \leq 1}} g_{z_0, \dots, z_K}(\beta). \quad (6)$$

To assess the quality of this approach, we compared our verification of nonclassicality with other methods. In Ref. [58], we demonstrated that a correlation matrix, M , obtained from the measured statistics in Eq. (1), is positive semidefinite for classical light, described through a nonnegative minimal eigenvalue μ_{\min} of M . The resulting notion of sub-multinomial light, $\mu_{\min} < 0$, was shown to be a better figure of merit than other means of verifying nonclassicality [59], such as sub-Poisson light [75, 76] and sub-binomial light [77, 78].

The comparison of g_{\min} and μ_{\min} for our data is shown in Table I for different heralding bins k_h . For the heralded one-photon (two-photon) state, we confirm $g_{\min} < 0$ with 9 (6) standard deviations, while the sub-multinomial behavior is less significant, 5 (3) standard deviations. Note that for the vacuum state, i.e., $k_h = 0$, both measures are consistent with the classical expectation, $g_{\min} = 0 = \mu_{\min}$.

V. RECONSTRUCTED DISTRIBUTIONS

From the data, we can directly estimate our DAPS distributions. The results of our extended analysis are shown in Fig. 2 and discussed in the following. Furthermore, we run the experiment twice: once with the signal blocked, and once with the signal unblocked.

To have full detector-agnostic approach, it is possible to define a detector-agnostic coherent amplitude,

$$|\beta^{(\text{DI})}\rangle = \sqrt{\sum_{N_0, \dots, N_K} [0N_0 + \dots + KN_K] c_{N_0, \dots, N_K}^{(\text{vac})}(\beta)}, \quad (7)$$

which is given by the statistics $c_{N_0, \dots, N_K}^{(\text{vac})}(\beta)$ measured by blocking the signal [60]. In case of photocounting, this gives $|\beta^{(\text{DI})}\rangle = \sqrt{\eta}|r|\beta\rangle$. As we do not record a phase, we consider full phase randomization. This does not affect the DAPS distributions of our heralded photon states. In Fig. 2, our DAPS distributions G_z are shown as a function of the amplitude in Eq. (7), determined through the vacuum measurement.

The same measurement renders it possible to theoretically predict the DAPS distribution of arbitrary states. Namely, a general DAPS distribution can be described as a convolution

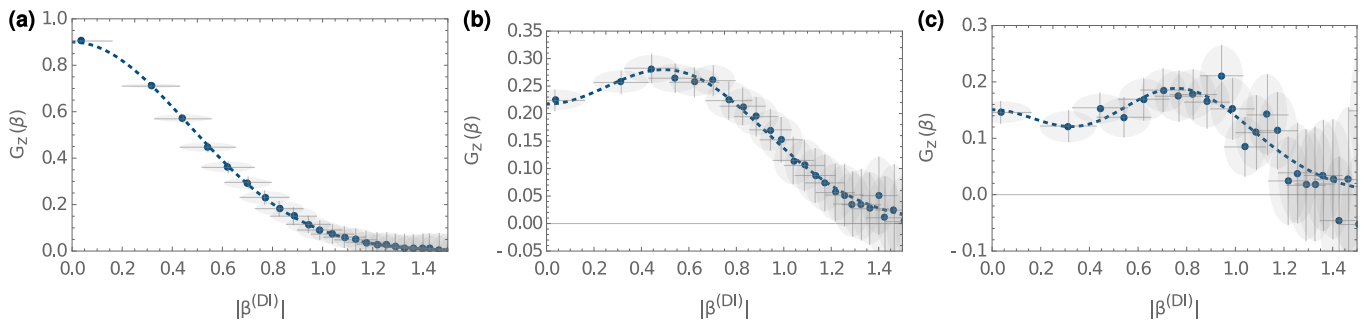


FIG. 2. Reconstructed DAPS distributions $G_z(\beta)$ [Eq. (4)] as a function of $|\beta^{(DI)}|$ [Eq. (7)]. We choose $z = -1.5$ as it would correspond to a Wigner function ($s = 0$) in the case of photocounting under the assumption of almost no loss, $\eta \approx 90\%$. From left to right, (a)–(c), heralded $k_h = 0, 1, 2$ -photon states are shown. The dashed lines correspond to the fit model inferred from the data obtained by blocking the signal [60]. The defining structures of the heralded (b) single-photon and (c) two-photon states are the oscillating patterns around the origin $|\beta^{(DI)}| = 0$.

of the measured vacuum distribution $G_z^{(\text{vac})}$ and the Glauber-Sudarshan distribution $P(\beta'; 1)$ of the state under study [60],

$$G_z(\beta) = \int d^2\beta' P(\beta'; 1) G_z^{(\text{vac})} \left(\beta - \frac{t}{r} \beta' \right). \quad (8)$$

In our case, the Gaussian shape of $G_z^{(\text{vac})}$ implies that heralded single-photon (two-photon) states should follow a Gaussian distribution multiplied with a first-order (second-order) polynomial in $|\beta^{(DI)}|^2$. In Fig. 2, this prediction (dashed lines) is confirmed as it correctly represents the DAPS distributions of the measured heralded photon states. The heralding to $k_h = 1$ gives a characteristic dip at the origin $|\beta^{(DI)}| = 0$, and the two-photon case, $k_h = 2$, leads to additional oscillations together with the appearance of a peak at the origin. We emphasize that the functional behavior $\beta \mapsto G_z(\beta)$ depends on the measurement operators, but the estimation of $G_z(\beta)$ is done independently of the detectors used, cf. first line in Eq. (2). Moreover, we are able to characterize defining features of other states without any other prior knowledge about the detectors from the data obtained using the vacuum state input [Eq. (8)].

Based on our reconstruction, we were able to determine a number of other properties of the produced states as well [60]. For instance, we can determine how well the DAPS distributions enable us to discern quantum states. For example, the single- and two-photon states [plots (b) and (c) in Fig. 2] can be distinguished from each other with more than 98% certainty. Furthermore, we can modify the z parameter which defines G_z . We found that for $z < -2.4$, the central dip of G_z [cf. Fig. 2(b)] becomes negative, similarly to the behavior of other known phase-space quasiprobability distributions. Our negativity has the highest statistical significance for $z = -4.85$, where $G_z(0) = -0.51 \pm 0.08$, being more than 6 standard deviations below the classical threshold of zero. This complements the results in Table I, based on $g_{z_0, \dots, z_K}(\beta) < 0$.

VI. SUMMARY AND DISCUSSION

We developed a theory and realized an experiment to characterize quantum light in phase space that functions for any

type of detector and without performing a prior detector characterization. Our theoretical framework is based on the generating function, defining our DAPS distribution, which can be directly estimated from measured correlations in a multiplexing setup. Moreover, we showed that our approach includes prominent phase-space quasiprobabilities as a special case. In addition, even more recent phase-space functions [79, 80], fundamentally restricted to on-off detectors, are encompassed by our technique.

In our proof-of-concept implementation, we demonstrated that a single multiplexing step is already sufficient to apply our DAPS distributions. This rendered it possible to verify the nonclassicality of multi-photon states, based on DAPS distributions, which resulted in greater statistical significance than obtained with earlier approaches [58, 59], which themselves already outperformed previous quantifiers of nonclassicality. Let us emphasize again that our nonclassicality criterion applies independently of the employed detectors. Furthermore, based on measuring vacuum as a reference, we were able to predict the defining phase-space features of heralded multi-photon states, which was then confirmed by directly reconstructing our DAPS distributions from our data. Our experiment comprises state-of-the-art detectors combined with an advantageous method to create coherent states, well mode-matched to our nonclassical signal. As our method is detector-agnostic, an efficiency budgeting becomes vastly meaningless; the number of data points merely has to be sufficient to produce statistically meaningful results.

For future applications, a measurement of the LO's phase would be interesting for applying our scheme to phase-sensitive nonclassical states, such as squeezed states. Furthermore, a generalization to infer nonclassicality with balanced homodyne detection and on-off detectors exists [81]. A similar technique could be used to generalize our results to other interferometric measurements in a detector-agnostic manner. In addition, we encounter the imperfections stemming from imbalances by assigning a corresponding systematic error. A possible bypass might include more sophisticated strategies, such as performed for the special case of binary detectors [82]. In conclusion, our detector-agnostic framework provides a universally applicable instrument for a robust char-

acterization of quantum light in phase space under challenging conditions and forms a basis for future research.

ACKNOWLEDGMENTS

The authors are grateful to William R. Clements for helpful discussions. The authors also thank Scott Glancy, Arik Avagyan, and Tim Bartley for valuable comments. The Integrated Quantum Optics group acknowledges financial support from the Gottfried Wilhelm Leibniz-Preis (Grant No. SII115/3-1). This work received funding through the Net-

worked Quantum Information Technologies (NQIT) hub (part of the UK National Quantum Technologies Programme) under Grant No. EP/N509711/1. G. S. T. acknowledges financial support from the Natural Sciences and Engineering Research Council of Canada and the Oxford Basil Reeve Graduate Scholarship. A. E. is supported by EPSRC (project EP/K034480/1 BLOQS). T. A. W. W. is supported by Fondation Wiener - Anspach. J. L. thanks the European Commission (H2020-FETPROACT-2014 grant QUCHIP). I. A. W. acknowledges ERC (Advanced Grant MOQUACINO). This work was supported by the Quantum Information Science Initiative (QISI).

-
- [1] M. Krenn, M. Malik, T. Scheidl, R. Ursin, and A. Zeilinger, *Quantum Communication with Photons*, in *Optics in Our Time* (Springer, Cham, 2016), pp. 455–482.
- [2] J. L. O’Brien, A. Furusawa, and J. Vučković, *Photonic quantum technologies*, *Nat. Phot.* **3**, 687 (2009).
- [3] T. C. Ralph and P. K. Lam, *A bright future for quantum communications*, *Nat. Phot.* **3**, 671 (2009).
- [4] D. F. Walls, *Squeezed states of light*, *Nature (London)* **306**, 141 (1983).
- [5] D. T. Smithey, M. Beck, M. G. Raymer, and A. Faridani, *Measurement of the Wigner distribution and the density matrix of a light mode using optical homodyne tomography: Application to squeezed states and the vacuum*, *Phys. Rev. Lett.* **70**, 1244 (1993).
- [6] G. Breitenbach, S. Schiller, and J. Mlynek, *Measurement of the quantum states of squeezed light*, *Nature (London)* **387**, 471 (1997).
- [7] A. I. Lvovsky, H. Hansen, T. Aichele, O. Benson, J. Mlynek, and S. Schiller, *Quantum State Reconstruction of the Single-Photon Fock State*, *Phys. Rev. Lett.* **87**, 050402 (2001).
- [8] G. Harder, C. Silberhorn, J. Rehacek, Z. Hradil, L. Motka, B. Stoklasa, and L. L. Sánchez-Soto, *Local Sampling of the Wigner Function at Telecom Wavelength with Loss-Tolerant Detection of Photon Statistics*, *Phys. Rev. Lett.* **116**, 133601 (2016).
- [9] T. Kiesel, W. Vogel, V. Parigi, A. Zavatta, and M. Bellini, *Experimental determination of a nonclassical Glauber-Sudarshan P function*, *Phys. Rev. A* **78**, 021804(R) (2008).
- [10] K. Laiho, Katiúscia N. Cassemiro, D. Gross, and C. Silberhorn, *Probing the Negative Wigner Function of a Pulsed Single Photon Point by Point*, *Phys. Rev. Lett.* **105**, 253603 (2010).
- [11] T. Douce, A. Eckstein, S. P. Walborn, A. Z. Khoury, S. Ducci, A. Keller, T. Coudreau, and P. Milman, *Direct measurement of the biphoton Wigner function through two-photon interference*, *Sci. Rep.* **3**, 3530 (2013).
- [12] C. Baune, J. Fiurášek, and R. Schnabel, *Negative Wigner function at telecommunication wavelength from homodyne detection*, *Phys. Rev. A* **95**, 061802(R) (2017).
- [13] D.-G. Welsch, W. Vogel, and T. Opatrny, *Homodyne Detection and Quantum-State Reconstruction*, *Prog. Opt.* **39**, 63 (1999).
- [14] C. Silberhorn, *Detecting quantum light*, *Contemp. Phys.* **48**, 143 (2007).
- [15] A. I. Lvovsky and M. G. Raymer, *Continuous-variable optical quantum-state tomography*, *Rev. Mod. Phys.* **81**, 299 (2009).
- [16] S. M. Tan, *An inverse problem approach to optical homodyne tomography*, *J. Mod. Opt.* **44**, 2233 (1997).
- [17] V. N. Starkov, A. A. Semenov, and H. V. Gomonay, *Numerical reconstruction of photon-number statistics from photocounting statistics: Regularization of an ill-posed problem*, *Phys. Rev. A* **80**, 013813 (2009).
- [18] T. Richter, *Pattern functions used in tomographic reconstruction of photon statistics revisited*, *Phys. Lett. A* **211**, 327 (1996).
- [19] U. Leonhard, M. Munroe, T. Kiss, T. Richter, and M. G. Raymer, *Sampling of photon statistics and density matrix using homodyne detection*, *Opt. Commun.* **127**, 144 (1996).
- [20] Z. Hradil, *Quantum-state estimation*, *Phys. Rev. A* **55**, R1561(R) (1997).
- [21] A. I. Lvovsky, *Iterative maximum-likelihood reconstruction in quantum homodyne tomography*, *J. Opt. B* **6**, S556 (2004).
- [22] J. Řeháček, D. Mogilevtsev, and Z. Hradil, *Operational Tomography: Fitting of Data Patterns*, *Phys. Rev. Lett.* **105**, 010402 (2010).
- [23] D. Mogilevtsev, A. Ignatenko, A. Maloshtan, B. Stoklasa, J. Rehacek, and Z. Hradil, *Data pattern tomography: reconstruction with an unknown apparatus*, *New J. Phys.* **15**, 025038 (2013).
- [24] P. L. Kelley and W. H. Kleiner, *Theory of electromagnetic field measurement and photoelectron counting*, *Phys. Rev.* **136**, A316 (1964).
- [25] M. Fleischhauer and D. G. Welsch, *Nonperturbative approach to multimode photodetection*, *Phys. Rev. A* **44**, 747 (1991).
- [26] A. K. Jaiswal and G. S. Agarwal, *Photoelectric Detection with Two-Photon Absorption*, *J. Opt. Soc. Am.* **59**, 1446 (1969).
- [27] M. K. Akhlaghi, A. H. Majedi, and J. S. Lundeen, *Nonlinearity in single photon detection: Modeling and quantum tomography*, *Opt. Express* **19**, 21305 (2011).
- [28] S. V. Polyakov and A. L. Migdall, *High accuracy verification of a correlated-photon-based method for determining photon-counting detection efficiency*, *Opt. Express* **15**, 1390 (2007).
- [29] A. P. Worsley, H. B. Coldenstrodt-Ronge, J. S. Lundeen, P. J. Mosley, B. J. Smith, G. Puentes, N. Thomas-Peter, and I. A. Walmsley, *Absolute efficiency estimation of photon-number-resolving detectors using twin beams*, *Opt. Express* **17**, 4397 (2009).
- [30] D. N. Klyshko, *Use of two-photon light for absolute calibration of photoelectric detectors*, *Sov. J. Quantum Electron.* **10**, 1112 (1980).
- [31] A. Luis and L. L. Sánchez-Soto, *Complete Characterization of Arbitrary Quantum Measurement Processes*, *Phys. Rev. Lett.* **83**, 3573 (1999).
- [32] J. Fiurášek, *Maximum-likelihood estimation of quantum measurement*, *Phys. Rev. A* **64**, 024102 (2001).

- [33] G. M. D’Ariano, L. Maccone, and P. Lo Presti, *Quantum Calibration of Measurement Instrumentation*, *Phys. Rev. Lett.* **93**, 250407 (2004).
- [34] A. Feito, J. S. Lundeen, H. Coldenstrodt-Ronge, J. Eisert, M. B. Plenio, and I. A. Walmsley, *Measuring measurement: Theory and practice*, *New J. Phys.* **11**, 093038 (2009).
- [35] H. B. Coldenstrodt-Ronge, J. S. Lundeen, K. L. Pregnell, A. Feito, B. J. Smith, W. Maurer, C. Silberhorn, J. Eisert, M. B. Plenio, and I. A. Walmsley, *A proposed testbed for detector tomography*, *J. Mod. Opt.* **56**, 432 (2009).
- [36] J. J. Renema, G. Frucci, Z. Zhou, F. Mattioli, A. Gaggero, R. Leoni, M. J. A. de Dood, A. Fiore, and M. P. van Exter, *Modified detector tomography technique applied to a superconducting multiphoton nanodetector*, *Opt. Express* **20**, 2806 (2012).
- [37] J. Peřina, Jr., O. Haderka, V. Michálek, and M. Hamar, *Absolute detector calibration using twin beams*, *Opt. Lett.* **37**, 2475 (2012).
- [38] M. Bohmann, R. Kruse, J. Sperling, C. Silberhorn, and W. Vogel, *Direct calibration of click-counting detectors*, *Phys. Rev. A* **95**, 033806 (2017).
- [39] K. E. Cahill and R. J. Glauber, *Density operators and quasiprobability distributions*, *Phys. Rev.* **177**, 1882 (1969).
- [40] G. S. Agarwal and E. Wolf, *Calculus for Functions of Noncommuting Operators and General Phase-Space Methods in Quantum Mechanics. II. Quantum Mechanics in Phase Space*, *Phys. Rev. D* **2**, 2187 (1970).
- [41] J. R. Klauder, *Improved Version of Optical Equivalence Theorem*, *Phys. Rev. Lett.* **16**, 534 (1966).
- [42] T. Kiesel and W. Vogel, *Nonclassicality filters and quasiprobabilities*, *Phys. Rev. A* **82**, 032107 (2010).
- [43] K. Husimi, *Some formal properties of the density matrix*, *Proc. Phys. Math. Soc. Jpn.* **22**, 264 (1940).
- [44] O. Landon-Cardinal, L. C. G. Govia, and A. A. Clerk, *Quantitative Tomography for Continuous Variable Quantum Systems*, *Phys. Rev. Lett.* **120**, 090501 (2018).
- [45] D. F. Mundarain and J. Stephany, *Husimi’s $Q(\alpha)$ function and quantum interference in phase space*, *J. Phys. A: Math. Gen.* **37**, 3869 (2004).
- [46] G. S. Agarwal, *Nonclassical characteristics of the marginals for the radiation field*, *Opt. Commun.* **95**, 109 (1993).
- [47] J. Park, Y. Lu, J. Lee, Y. Shen, K. Zhang, S. Zhang, M. S. Zubairy, K. Kim, and H. Nha, *Revealing nonclassicality beyond Gaussian states via a single marginal distribution*, *Proc. Natl. Acad. Sci. U.S.A.* **114**, 891 (2017).
- [48] J. Sperling and I. A. Walmsley, *Quasiprobability representation of quantum coherence*, *Phys. Rev. A* **97**, 062327 (2018).
- [49] G. S. Agarwal, *Relation between atomic coherent-state representations, state multipoles, and generalized phase-space distributions*, *Phys. Rev. A* **24**, 2889 (1981).
- [50] J. P. Dowling, G. S. Agarwal, and W. P. Schleich, *Wigner distribution of a general angular-momentum state: Applications to a collection of two-level atoms*, *Phys. Rev. A* **49**, 4101 (1994).
- [51] R. McConnell, H. Zhang, J. Hu, S. Ćuk, and V. Vuletić, *Entanglement with negative Wigner function of almost 3,000 atoms heralded by one photon*, *Nature (London)* **519**, 439 (2015).
- [52] D. Leibfried, D. M. Meekhof, B. E. King, C. Monroe, W. M. Itano, and D. J. Wineland, *Experimental Determination of the Motional Quantum State of a Trapped Atom*, *Phys. Rev. Lett.* **77**, 4281 (1996).
- [53] A. Sanpera, R. Tarrach, and G. Vidal, *Local description of quantum inseparability*, *Phys. Rev. A* **58**, 826 (1998).
- [54] J. Sperling and W. Vogel, *Representation of entanglement by negative quasiprobabilities*, *Phys. Rev. A* **79**, 042337 (2009).
- [55] J. Sperling, E. Meyer-Scott, S. Barkhofen, B. Brecht, and C. Silberhorn, *Experimental Reconstruction of Entanglement Quasiprobabilities*, *Phys. Rev. Lett.* **122**, 053602 (2019).
- [56] S. Wallentowitz and W. Vogel, *Unbalanced homodyning for quantum state measurements*, *Phys. Rev. A* **53**, 4528 (1996).
- [57] H. Paul, P. Törmä, T. Kiss, and I. Jex, *Photon Chopping: New Way to Measure the Quantum State of Light*, *Phys. Rev. Lett.* **76**, 2464 (1996).
- [58] J. Sperling, W. R. Clements, A. Eckstein, M. Moore, J. J. Renema, W. S. Kolthammer, S. W. Nam, A. Lita, T. Gerrits, W. Vogel, G. S. Agarwal, and I. A. Walmsley, *Detector-Independent Verification of Quantum Light*, *Phys. Rev. Lett.* **118**, 163602 (2017).
- [59] J. Sperling, A. Eckstein, W. R. Clements, M. Moore, J. J. Renema, W. S. Kolthammer, S. W. Nam, A. Lita, T. Gerrits, I. A. Walmsley, G. S. Agarwal, and W. Vogel, *Identification of nonclassical properties of light with multiplexing layouts*, *Phys. Rev. A* **96**, 013804 (2017).
- [60] See the Supplemental Material (pp. 7) for technical details about the experiment and theory, the data and error analysis, and additional results.
- [61] R. J. Glauber, *Coherent and incoherent states of the radiation field*, *Phys. Rev.* **131**, 2766 (1963).
- [62] E. C. G. Sudarshan, *Equivalence of Semiclassical and Quantum Mechanical Descriptions of Statistical Light Beams*, *Phys. Rev. Lett.* **10**, 277 (1963).
- [63] U. M. Titulaer and R. J. Glauber, *Correlation functions for coherent fields*, *Phys. Rev.* **140**, B676 (1965).
- [64] L. Mandel, *Non-classical states of the electromagnetic field*, *Phys. Scr.* **T12**, 34 (1986).
- [65] W. Vogel and D.-G. Welsch, *Quantum Optics* (Wiley-VCH, Weinheim, 2006).
- [66] G. S. Agarwal, *Quantum Optics* (Cambridge University Press, 2012).
- [67] E. Wolf and C. L. Mehta, *Determination of the Statistical Properties of Light from Photoelectric Measurements*, *Phys. Rev. Lett.* **13**, 705 (1964).
- [68] Note that in our case, the z parameter is not limited to values that correspond to $-1 \leq s \leq 1$ because of \mathcal{A} being a finite set and, thus, guaranteeing convergence of G_z for any z .
- [69] A. Eckstein, A. Christ, P. J. Mosley, and C. Silberhorn, *Highly Efficient Single-Pass Source of Pulsed Single-Mode Twin Beams of Light*, *Phys. Rev. Lett.* **106**, 013603 (2011).
- [70] M. Liscidini and J. E. Sipe, *Stimulated Emission Tomography*, *Phys. Rev. Lett.* **111**, 193602 (2013).
- [71] A. E. Lita, A. J. Miller, and S.W. Nam, *Counting near infrared single-photons with 95% efficiency*, *Opt. Express* **16**, 3032 (2008).
- [72] P. C. Humphreys, B. J. Metcalf, T. Gerrits, T. Hiemstra, A. E. Lita, J. Nunn, S. W. Nam, A. Datta, W. S. Kolthammer, and I. A. Walmsley, *Tomography of photon-number resolving continuous-output detectors*, *New J. Phys.* **17**, 103044 (2015).
- [73] R. P. Welty and J. M. Martinis, *A series array of DC SQUIDS*, *IEEE Trans. Magn.* **27**, 2924 (1991).
- [74] E. Figueroa-Feliciano, B. Cabrera, A. J. Miller, S. F. Powell, T. Saab, and A. B. C. Walker, *Optimal filter analysis of energy-dependent pulse shapes and its application to TES detectors*, *Nucl. Instrum. Methods Phys. Res. A* **444**, 453 (2000).
- [75] L. Mandel, *Sub-Poissonian photon statistics in resonance fluorescence*, *Opt. Lett.* **4**, 205 (1979).
- [76] R. Short and L. Mandel, *Observation of Sub-Poissonian Photon Statistics*, *Phys. Rev. Lett.* **51**, 384 (1983).
- [77] J. Sperling, W. Vogel, and G. S. Agarwal, *Sub-Binomial Light*, *Phys. Rev. Lett.* **109**, 093601 (2012).

- [78] T. J. Bartley, G. Donati, X.-M. Jin, A. Datta, M. Barbieri, and I. A. Walmsley, *Direct Observation of Sub-Binomial Light*, *Phys. Rev. Lett.* **110**, 173602 (2013).
- [79] A. Luis, J. Sperling, and W. Vogel, *Nonclassicality Phase-Space Functions: More Insight with Fewer Detectors*, *Phys. Rev. Lett.* **114**, 103602 (2015).
- [80] M. Bohmann, J. Tiedau, T. Bartley, J. Sperling, C. Silberhorn, and W. Vogel, *Incomplete Detection of Nonclassical Phase-*

Space Distributions, *Phys. Rev. Lett.* **120**, 063607 (2018).

- [81] J. Sperling, W. Vogel, and G. S. Agarwal, *Balanced homodyne detection with on-off detector systems: Observable nonclassicality criteria*, *Europhys. Lett.* **109**, 34001 (2015).
- [82] C. Lee, S. Ferrari, W. H. P. Pernice, and C. Rockstuhl, *Sub-Poisson-binomial light*, *Phys. Rev. A* **94**, 053844 (2016).
- [83] J. Sperling, W. Vogel, and G. S. Agarwal, *Quantum state engineering by click counting*, *Phys. Rev. A* **89**, 043829 (2014).

SUPPLEMENTAL MATERIAL

Appendix A: Details on the experiment

The experimental setup is shown in Fig. 3. Our pump laser is a titanium sapphire (Ti:Saph) regenerative amplifier that generates femtosecond pulses (center wavelength 780 nm, full width at half maximum [FWHM] 15 nm) at a rate of 100 kHz. This rate is chosen to accommodate the thermal relaxation time ($\sim 10 \mu\text{s}$) of the transition-edge sensors (TESs). We split the pulses into two paths, each pumping a periodically poled potassium titanyl phosphate (ppKTP) waveguide.

We pump the first waveguide (right in Fig. 3) using filtered (center 775 nm, FWHM 2 nm) pulses from the Ti:Saph. Pumping the ppKTP waveguide generates two-mode squeezed vacuum via type-II parametric down-conversion. The pump is then discarded using a longpass filter. The two down-converted modes (signal 1554 nm, idler 1547 nm) are orthogonally polarized and separated by a polarisation beam splitter. Each mode is sent through a bandpass filter (FWHM 10 nm). The idler mode is sent to a TES detector to herald photon-number states in the signal mode (heralding efficiency $\sim 40\%$) by postselecting to a specific outcome k_h .

In the second waveguide (left in Fig. 3), we prepare the local oscillator (LO). Since the first and second waveguides have slightly different phase-matching properties, a different pump spectrum (center 783 nm, FWHM 2 nm) is used. This pump spectrum is chosen to maximize the spectral overlap between the LO and signal (SI). We also carve 2 ns square seed pulses from a continuous-wave laser (center 1580 nm) using an electro-optic modulator. The pump and seed pulses are temporally overlapped and coupled into the second ppKTP waveguide. Through difference frequency generation, the LO is generated in the polarization orthogonal to the seed. The LO is separated from the seed using a polarisation beam splitter. As before, we discard the pump by a longpass filter. The LO's polarization is adjusted with a half-wave plate to match the SI's polarization. Then, the LO is sent through a bandpass filter (FWHM 10 nm) to further eliminate seed light as well as increase the spectral overlap with the signal. Finally, neutral-density filters attenuate the LO to the single-photon level.

The SI and LO are combined on a 90:10 beam splitter. The resulting light field of one output then enters the multiplexing step (50:50 beam splitter) and the then resulting beams are measured with two TESs. The recorded coincidences give the detection events $E(k_1, k_2)$, which we use for our analysis.

In addition, we characterized the mode overlap of the signal and LO by combining the two on a 50:50 beam splitter. We

consider the specific case of a single photon ($k_h = 1$) and a weak LO ($|\beta| \ll 1$). By scanning the delay between the SI and LO, we expect to measure a Hong-Ou-Mandel-type dip in two-fold coincidences at the output of the beam splitter. We measured a dip of $\sim 80\%$ visibility, suggesting that the mode overlap is at least 80%. By blocking the signal, this setup constitutes a Hanbury Brown-Twiss interferometer that allows us to measure the LO's $g^{(2)}(0)$. We measured $g^{(2)}(0) = 1.005 \pm 0.002$, which is consistent with the expected Poisson distribution for the LO's photon statistics.

Appendix B: Details on the theory

1. General approach

Let us formulate some additional details on the theory. As we can expand any SI state in the Glauber-Sudarshan decom-

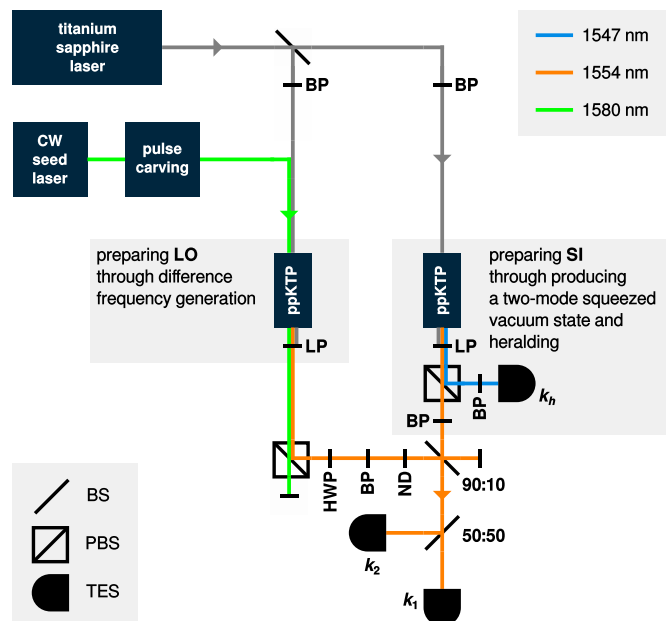


FIG. 3. Outline of the setup; see Sec. A for the full description. BP: bandpass filter, BS: beam splitter, CW: continuous-wave, HWP: half-wave plate, ppKTP: periodically poled potassium titanyl phosphate, LP: longpass filter, ND: neutral-density filter, PBS: polarizing beam splitter, TES: transition-edge sensor.

position, $\hat{\rho} = \int d^2\alpha P(\alpha)|\alpha\rangle\langle\alpha|$, it is sufficient to consider the propagation of coherent states $|\alpha\rangle$. Our detection scheme consists of a combination of the SI with the LO state $|\beta\rangle$ on a beam splitter, the multiplexing, and the detection.

Applying a beam splitter transformation, we map an input, consisting of SI and LO, as follows: $|\alpha\rangle \otimes |\beta\rangle \mapsto |t\alpha - r\beta\rangle \otimes |r^*\alpha + t^*\beta\rangle$, where t and r define the transmissivity and reflectivity ($|t|^2 + |r|^2 = 1$). When tracing over the second mode, we obtain the state that enters the multiplexing stage,

$$\hat{\rho}(\beta) = \int d^2\alpha P(\alpha)|t\alpha - r\beta\rangle\langle t\alpha - r\beta|. \quad (\text{B1})$$

Further, the multiplexing distributes the coherent state components in Eq. (B1) among the $N = 2^S$ output beams, where S is the depth of the multiplexing scheme, $|\gamma\rangle \mapsto |\gamma/\sqrt{N}\rangle^{\otimes N}$, resulting in $\int d^2\alpha P(\alpha)[|(t\alpha - r\beta)/\sqrt{N}\rangle\langle(t\alpha - r\beta)/\sqrt{N}|]^{\otimes N}$. Using some combinatorics (see Ref. [59] for details), we find

$$c_{N_0, \dots, N_K}(\beta) = \int d^2\alpha P(\alpha) \frac{N!}{N_0! \dots N_K!} \times \prod_{k=0}^K \underbrace{\left\langle \frac{t\alpha - r\beta}{\sqrt{N}} \left| \hat{\pi}_k \right| \frac{t\alpha - r\beta}{\sqrt{N}} \right\rangle^{N_k}}_{\stackrel{\text{def.}}{=} p_k \left(\frac{t\alpha - r\beta}{\sqrt{N}} \right)}, \quad (\text{B2})$$

where $\{\hat{\pi}_k\}_{k=0, \dots, K}$ is an unknown positive operator-valued measure (POVM) that describes the detector.

Consequently, the two types of generating functions under consideration read

$$g_{z_0, \dots, z_K}(\beta) = \int d^2\alpha P(\alpha) \left[\sum_{k=0}^K z_k p_k \left(\frac{t\alpha - r\beta}{\sqrt{N}} \right) \right]^N \quad (\text{B3})$$

and

$$G_z(\beta) = \int d^2\alpha P(\alpha) \left[\sum_{k=0}^K z^k p_k \left(\frac{t\alpha - r\beta}{\sqrt{N}} \right) \right]^N, \quad (\text{B4})$$

using the Glauber-Sudarshan P function. As long as N is even and $P \geq 0$, both expressions are necessarily nonnegative.

2. Photoelectric counting with loss

Let us analyze our scheme for the special case of photoelectric counting. A simple photoelectric detection is described through POVM elements $\hat{\pi}_k = :e^{-\eta\hat{n}}(\eta\hat{n})^k/k!:$ for $k = 0, 1, \dots$ ($K = \infty$), where η is the quantum efficiency and \hat{n} is the photon-number operator. In this scenario, the generating function in Eq. (B4) can be further evaluated [67] and reads

$$G_z(\beta) = \int d^2\alpha P(\alpha) \exp\left(-[1-z]|t|^2\eta\left|\alpha - \frac{r}{t}\beta\right|^2\right) = \left\langle : \exp\left[-(1-z)|t|^2\eta\hat{n}\left(\frac{r}{t}\beta\right)\right] : \right\rangle_{\hat{\rho}}, \quad (\text{B5})$$

where $\hat{n}(\gamma)$ is the displaced photon-number operator. Since we have $P(\gamma; s) = 2(\pi[1-s])^{-1} \langle :e^{-2\hat{n}(\gamma)/(1-s)}: \rangle_{\hat{\rho}}$ [56], the above expression can be related to s -parameterized distributions.

Also note that according to the characterization performed in Ref. [59] (Sec. III), our TESSs are more precisely described through POVMs of the form $\hat{\pi}_k = :e^{-\Gamma(\hat{n})}\Gamma(\hat{n})^k/k!:$ for $k = 0, \dots, K-1$ and $\hat{\pi}_K = \hat{1} - \sum_{k=0}^{K-1} \hat{\pi}_k$. Therein, $K < \infty$ reflects the finite photon-number resolution, and the response function Γ has a nonlinear form, $\Gamma(\hat{n}) \approx \eta\hat{n} + \eta^{(2)}\hat{n}^2$, where the quantum efficiency η is not one ($\eta < 1$) and the nonlinear contribution does not vanish ($\eta^{(2)} \neq 0$). As $\eta^{(2)}$ is small, the nonlinear behavior mainly affects higher LO and SI intensities.

Appendix C: Coincidences and systematic errors

A single multiplexing step, $N = 2$, was implemented. Thus, it is convenient to formulate the data processing in terms of measured coincidences. For this purpose, we denote with $E(k_1, k_2)$ the number of coincidence events for the measurement outcomes k_1 and k_2 ($k_1, k_2 \in \{0, \dots, K\}$), resembling the detection bins of the TESSs 1 and 2, respectively. $E = \sum_{k_1, k_2} E(k_1, k_2)$ defines the total number of events.

The coincidences are directly related to the desired quantum version of a multinomial distribution, c_{N_0, \dots, N_K} , cf. Eq. (1) in the main text. Since $N_0 + \dots + N_K = N = 2$, we have

$$c_{N_0, \dots, N_K} = \begin{cases} c_{0, \dots, 0, N_i=2, 0, \dots, 0} & \text{for } 0 \leq i \leq K, \\ c_{0, \dots, 0, N_i=1, 0, \dots, 0, N_j=1, 0, \dots, 0} & \text{for } 0 \leq i < j \leq K, \\ 0 & \text{otherwise,} \end{cases} \quad (\text{C1})$$

where we can identify $c_{0, \dots, 0, N_i=2, 0, \dots, 0} = E(i, i)/E$ and $c_{0, \dots, 0, N_i=1, 0, \dots, 0, N_j=1, 0, \dots, 0} = (E(i, j) + E(j, i))/E$. To estimate the value \bar{f} of a function f_{N_0, \dots, N_K} , we can recast the standard sampling formula as follows:

$$\begin{aligned} \bar{f} &= \sum_{\substack{N_0, \dots, N_K: \\ N_0 + \dots + N_K = N}} f_{N_0, \dots, N_K} c_{N_0, \dots, N_K} \\ &= \sum_{0 \leq i \leq K} \frac{E(i, i)}{E} \overbrace{f_{0, \dots, 0, N_i=2, 0, \dots, 0}}^{\stackrel{\text{def.}}{=} f(i, i)} \\ &\quad + \sum_{0 \leq i < j \leq K} \frac{E(i, j) + E(j, i)}{E} \underbrace{f_{0, \dots, 0, N_i=1, 0, \dots, 0, N_j=1, 0, \dots, 0}}_{\stackrel{\text{def.}}{=} f(i, j) = f(j, i)} \\ &= \frac{1}{E} \sum_{i, j=0}^K f(i, j) E(i, j). \end{aligned} \quad (\text{C2})$$

See the Supplemental Material to Ref. [58] for the generalization to $N > 2$.

In order to apply the multinomial framework described in the main text, one has to satisfy the premise that the coincidence statistics is symmetric, $E(k_1, k_2) = E(k_2, k_1)$. However, in reality, this is only true to a limited extent since the beam splitters in the multiplexing might not be perfectly balanced,

and the detectors after the multiplexing might have slightly different responses. In Ref. [58], we provided a rough systematic error estimate to account for such imperfections, which is further refined in the following.

The premises mentioned above state that the coincidences are symmetric. The actual measurements $E(k_1, k_2)$ naturally exhibit a certain amount of asymmetry; if not, no systematic error needs to be assigned. We can decompose the coincidences as follows:

$$E(k_1, k_2) = \frac{\overbrace{E(k_1, k_2) + E(k_2, k_1)}^{\text{(symmetric part)}}}{2} + \frac{\overbrace{E(k_1, k_2) - E(k_2, k_1)}^{\text{(asymmetric part)}}}{2}. \quad (\text{C3})$$

Furthermore, assume we estimate a function $f(k_1, k_2)$ to obtain the mean $\bar{f} = \sum_{k_1, k_2} f(k_1, k_2) E(k_1, k_2) / E$. Inserting the above decomposition and denoting with $\bar{f}^{(\text{sym})}$ the value obtained from the symmetric part in Eq. (C3), we apply the triangle inequality and find

$$\left| \bar{f} - \bar{f}^{(\text{sym})} \right| \leq \sum_{k_1, k_2} |f(k_1, k_2)| \left| \frac{E(k_1, k_2) - E(k_2, k_1)}{2E} \right| = \varepsilon_f, \quad (\text{C4})$$

which is the systematic error resulting from the asymmetry in the measured data.

As we use the typical quadratic error propagation—rather than the linear form used for the above derivation—, we replace the right-hand-side expression in Eq. (C4) with $\varepsilon_f^2 = \sum_{k_1, k_2} |f(k_1, k_2)|^2 [E(k_1, k_2) - E(k_2, k_1)]^2 / [2E]^2$. Recall that the general relation between linear and quadratic error expansion for a function $F(x_1, x_2, \dots)$ is given by $\Delta^{(\text{lin})} F = \sum_j |\partial F / \partial x_j| \Delta x_j$ and $\Delta^{(\text{quad})} F = (\sum_j |\partial F / \partial x_j|^2 [\Delta x_j]^2)^{1/2}$. In addition, let us remind ourselves that the random error reads $\sigma_f = [(\bar{f}^2 - \bar{f}^2) / (E - 1)]^{1/2}$, which is combined with the systematic error to give the overall uncertainty, $\Delta f = \sqrt{\varepsilon_f^2 + \sigma_f^2}$.

Appendix D: Sub-multinomial light

We assess our results with our previously derived nonclassicality criteria [58, 59]. Let us briefly recapitulate this approach and its implementation for a self-consistent reading. The previously devised method is based on the observation that a correlation matrix, M , is positive semidefinite for classical light, i.e., $M = (M_{i,j})_{i,j=0,\dots,K} \geq 0$, where

$$M_{i,j} = N \overline{N_i(N_j + \delta_{i,j})} - (N-1) \overline{N_i} \overline{N_j} = N^2(N-1) (\langle : \hat{\pi}_i \hat{\pi}_j : \rangle - \langle \hat{\pi}_i : \rangle \langle \hat{\pi}_j : \rangle), \quad (\text{D1})$$

with δ denoting the Kronecker symbol. It was shown that the required first- and second-order moments can be obtained

TABLE II. For the available heralding bins, k_h , the minimal eigenvalues μ_{\min} of the matrix M are shown. Significant negativities defines the notion of nonclassical sub-multinomial light [58, 59].

k_h	sub-multinomial
0	-0.0000 ± 0.0009
1	-0.15 ± 0.03
2	-0.10 ± 0.03
3	-0.17 ± 0.07
4	-0.3 ± 0.2

from coincidences as [58]

$$\overline{N_i} = N \langle : \hat{\pi}_i : \rangle = \sum_{k_1, k_2} (\delta_{k_1, i} + \delta_{k_2, i}) \frac{E(k_1, k_2)}{E}, \quad (\text{D2})$$

$$\overline{N_i(N_j + \delta_{i,j})} = N(N-1) \langle : \hat{\pi}_i \hat{\pi}_j : \rangle$$

$$= \sum_{k_1, k_2} (\delta_{k_1, i} \delta_{k_2, j} + \delta_{k_1, j} \delta_{k_2, i}) \frac{E(k_1, k_2)}{E}. \quad (\text{D3})$$

Finally, the minimal eigenvalue μ_{\min} of the correspondingly reconstructed matrix M is computed to probe for positive semidefiniteness.

The heralding with a TES enables us to generate higher-order photon-number states. In Table II, we listed the nonclassicality in terms of the criteria $\mu_{\min} < 0$ for data with a coherent amplitude zero. The observed nonclassicality in Table II for heralding bins larger than two is no longer significant within a three-standard-deviation error margin as the total number of events E is too small in those cases. For this reason, we restrict our considerations to heralding bins $k_h \in \{0, 1, 2\}$.

Appendix E: Local oscillator amplitudes

From the first derivative of Eq. (B5) for the photoelectric model, we can infer the dimensionless and displaced intensity,

$$I(\beta) = \left. \frac{\partial G_z(\beta)}{\partial z} \right|_{z=1} = |t|^2 \eta \langle : \hat{n} \left(\frac{r}{t} \beta \right) : \rangle_{\hat{\rho}} \quad (\text{E1})$$

$$= \sum_{\substack{N_0, N_1, \dots \geq 0: \\ N_0 + N_1 + \dots = N}} (0N_0 + 1N_1 + \dots) c_{N_0, \dots, N_K}(\beta),$$

where the latter expression results from the definition $G_z(\beta) = \sum_{N_0, N_1, \dots} z^{0N_0 + 1N_1 + \dots} c_{N_0, \dots, N_K}(\beta)$. Most importantly, in the case that the SI is vacuum, we find $\langle : \hat{n}(\gamma) : \rangle_{|0\rangle\langle 0|} = |\gamma|^2$. We abstract this observation and define for the general detection scenario a detector-independent amplitude $|\beta^{(\text{DI})}| = \sqrt{I(\beta)} = \sqrt{\partial G_z(\beta) / \partial z}|_{z=1}$ for general POVMs and the SI $\hat{\rho} = |0\rangle\langle 0|$. This also explains the following Eq. (E2) as well as Eq. (7) in the main text.

We block the SI to infer the amplitude of the LO. The intensity, here represented through the dimensionless quantity

$$\left| \beta^{(\text{DI})} \right|^2 = \sum_{i=0}^K i \overline{N_i} \in [0, NK], \quad (\text{E2})$$

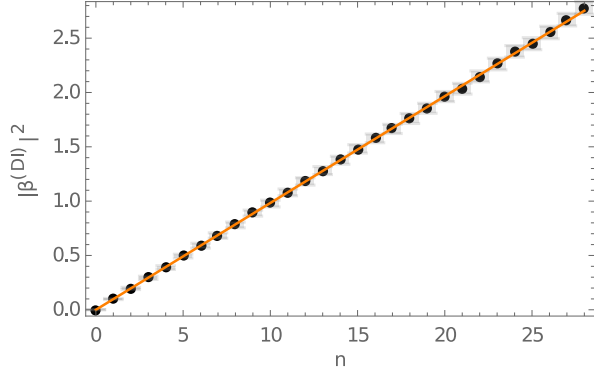


FIG. 4. The estimated intensity [cf. Eq. (E2)] as a function of the used setting number n . The slope of the linear fit (orange line) is 0.1. This confirms the intended difference of 1 photon between two settings when correcting for the 90 : 10 splitting that uses 10% of the LO intensity.

has been varied, realized via $n = 0, \dots, 28$ power settings of the seed laser. These settings have been also applied when the SI is not blocked. The settings are chosen such that an equidistant intensity grid is generated. This is confirmed through the linear fit in Fig. 4.

Appendix F: Additional analysis and results

1. Typical data and error estimates

In order to further assess the impact of uncertainties, let us consider a typical example. In Fig. 5, we depict a typical data set, there for a single photon (i.e., heralding to bin $k_h = 1$) and a vanishing LO amplitude (i.e., the setting $n = 0$).

The resulting (systematic and random) observational errors for the generating function are depicted in Fig. 6. The expected trend of monotonicity and the diverging behavior of the uncertainties as a function of $|z|$ are clearly visible. As $G_{z=1}(\beta) = 1$ corresponds to the total probability, which is not subject to fluctuations, the random error vanishes for $z = 1$ (Fig. 6, top-left panel). By construction, the systematic errors are symmetric with respect to $z = 0$ (top-right plot in Fig. 6). See also the following discussion in Sec. F2.

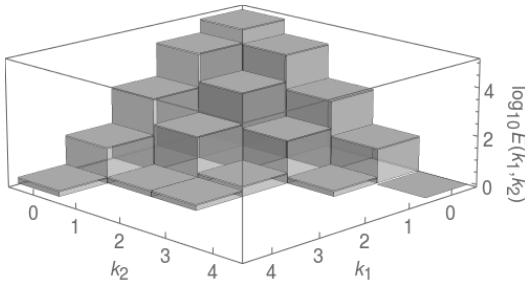


FIG. 5. Raw coincidence data for $k_h = 1$ and $\beta = 0$. We recorded $E = 184426$ events in $K + 1 = 5$ bins.

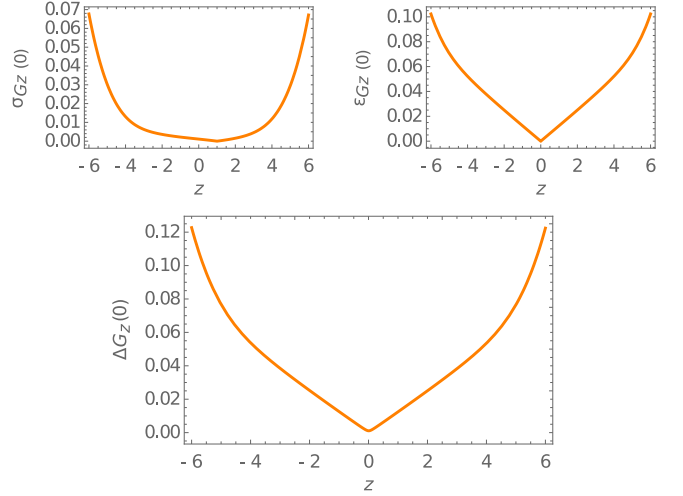


FIG. 6. Error composition for the sampling of $G_z(\beta = 0)$ as a function of z for the data shown in Fig. 5 [top-left: random error, $\sigma_{G_z(0)}$; top-right: systematic error, $\epsilon_{G_z(0)}$; bottom: combination of both random and systematic uncertainties, $\Delta G_z(0)$].

For probing the nonclassicality through the generating function, obtained as $g_{z_0, \dots, z_K}(\beta) = \sum_{k_1, k_2} z_{k_1} z_{k_2} E(k_1, k_2)/E$, we compute the eigenvector $Z = [z_0, \dots, z_K]$ to the normalized coincidence matrix $[E(k_1, k_2)/E]_{k_1, k_2=0, \dots, K}$ that corresponds to the minimal eigenvalue. For the example under study, we get $Z = [0.228, -0.973, -0.033, -0.001, -0.000]$. With this information, we can now estimate the general generating function and get $g_{z_0, \dots, z_K}(\beta) = -0.026 \pm 0.003$ as the optimal negativity, here for $\beta = 0$. The minimum over all measured LO amplitudes then yields g_{\min} , cf. Eq. (6) in the main text.

2. Optimal quasiprobability distribution and error estimates

We found that the parameter $z = -4.85$ is optimal in the sense that $G_z(\beta)$ has the most statistically significant negativity at the origin (see Fig. 7), i.e., $-G_z(0)/\Delta G_z(0)$ is maximized. In the plotted scenario, the error estimates $\Delta G_z(\beta)$ are rapidly increasing for increasing $|\beta|$, which we discuss in the following based on the sampling formula

$$G_z(\beta) = \sum_{N_0 + \dots + N_K = N} z^{0N_0 + \dots + KN_K} c_{N_0, \dots, N_K}(\beta). \quad (\text{F1})$$

For increasing LO amplitudes, the components of $c_{N_0, \dots, N_K}(\beta)$ that relate to a higher power of z have a higher contribution to the estimate of this function. Similarly, $|z| > 1$ also leads to a most relevant term that corresponds to a higher power of z . Recall that the exponent $0N_0 + \dots + KN_K$ relates to the overall intensity [cf. Eq. (E2)]. Consequently, both a large LO amplitude and $|z| > 1$ result in the fact that the contribution for z^p for larger p becomes the most relevant one. Standard error propagation then implies a relative error scaled by the large factor p , for increasing LO amplitudes and increasing $|z|$ values, which also explains why the increase of observational uncertainties in those scenarios is expected.

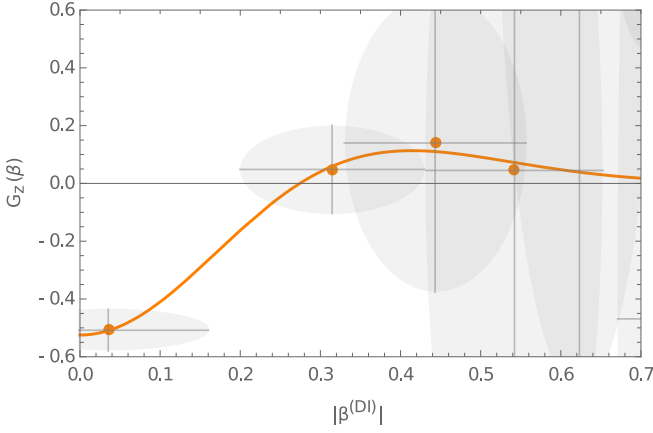


FIG. 7. Radial component of the phase-space distribution of the heralded single-photon state ($k_h = 1$) for the optimal value $z = -4.85$. For almost all data points with $|\beta^{(DI)}| > \sqrt{0.5}$, the error estimates exceeds the plot range while allowing for consistency with expected mean values close to zero, cf. the discussion in Sec. F.2.

Appendix G: Quantum state discrimination

As our distributions can, in principle, take arbitrary forms for arbitrary detectors, let us formulate the statistical model to discriminate states based on the reconstructed phase-space functions alone. The probability that two distributions, described through multivariate random variables X and X' , are indistinguishable within a δ -uncertainty can be expressed as

$$\text{Prob}(|X - X'| \leq \delta) = \int_{-\delta}^{+\delta} du \int_{-\infty}^{+\infty} dz p(X = z) p(X' = z + u), \quad (\text{G1})$$

where $p(X)$ and $p(X')$ are the probability densities of the uncertainties for the two random variables. We identify $X = [G_z^{(k_h)}(\beta_0), \dots, G_z^{(k_h)}(\beta_{28})]$ and $X' = [G_z^{(k'_h)}(\beta_n)]_{n=0, \dots, 28}$ for different heralded states and LO settings and use a Gaussian error model with a mean and variance that corresponds to the reconstructed distributions for each measured setting n . Consequently, we get from Eq. (G1) the following probability for the discrimination:

$$\begin{aligned} \text{Prob}(G_z^{(k_h)} \neq G_z^{(k'_h)}) &= 1 - \text{Prob}(\forall n : |X_n - X'_n| \leq \delta_n) \\ &= 1 - \prod_n \underbrace{\int_{-\delta_n}^{+\delta_n} du_n \frac{\exp\left[-\frac{(u_n - [\mu_n - \mu'_n])^2}{2\Delta_n^2}\right]}{\sqrt{2\pi\Delta_n^2}}}_{=\text{Err}\left[\frac{|\mu_n - \mu'_n|}{\Delta_n} + 3\right] - \text{Err}\left[\frac{|\mu_n - \mu'_n|}{\Delta_n} - 3\right]}, \end{aligned} \quad (\text{G2})$$

where we set the vector δ to correspond to three combined standard deviations for each setting, $\delta_n = 3\Delta_n$ and $\Delta_n = [\Delta G_z^{(k_h)}(\beta_n)^2 + \Delta G_z^{(k'_h)}(\beta_n)^2]^{1/2}$, and using the mean values $\mu_n = G_z^{(k_h)}(\beta_n)$ and $\mu'_n = G_z^{(k'_h)}(\beta_n)$. Note that $\text{Err}[z] = \int^z d\xi e^{-\xi^2/2} / \sqrt{2\pi}$ denotes the error function.

For instance, we find for our measured data that the likelihood to discriminate the phase-space distributions for k_h from the one for k'_h for $z = -1.5$ is given by the matrix

$$\left[\text{Prob}(G_z^{(k_h)} \neq G_z^{(k'_h)}) \right]_{k_h, k'_h=0,1,2} = \begin{bmatrix} 7.5\% & 100.\% & 100.\% \\ 100.\% & 7.5\% & 98.9\% \\ 100.\% & 98.9\% & 7.5\% \end{bmatrix}, \quad (\text{G3})$$

where “100.%” corresponds to a value which is 100% within the used numerical precision. Note that the diagonal elements are nonzero as identical distributions could still represent different states when considering a finite error margin.

Appendix H: Fit model from vacuum measurements

From the measurement in which the SI is blocked (i.e., vacuum SI), we can extrapolate the general shape of the phase-space distribution for photon states, without relying on any particular detector model. This approach is also used to fit the reconstructed distributions for the heralding to k_h .

Using the data where the signal is blocked, we find that a Gaussian distribution describes the reconstructed phase-space distribution for vacuum quite well; see Fig. 8. This information can be used to predict the phase-space distributions of m -photon states as well. Because of Eq. (B4) and the known representation $P^{(m)}(\alpha) = \sum_{j=0}^m \binom{m}{j} j!^{-1} \partial_\alpha^j \partial_{\alpha^*}^j P^{(0)}(\alpha)$ [65], where $P^{(0)}(\alpha)$ describes the delta distribution centered at the origin, we find that the m -th photon state is given by

$$G_z^{(m)}(\beta) = \sum_{j=0}^m \binom{m}{j} \frac{1}{j!} \left[\frac{|t|^2}{|r|^2} \right]^j \partial_\beta^j \partial_{\beta^*}^j G_z^{(0)}(\beta), \quad (\text{H1})$$

where $G_z^{(0)}(\beta)$ is experimentally obtained by blocking the signal (Fig. 8) and which is determined without relying on any detection models. For deriving Eq. (H1), note that the argument of the vacuum function implies that a partial integration

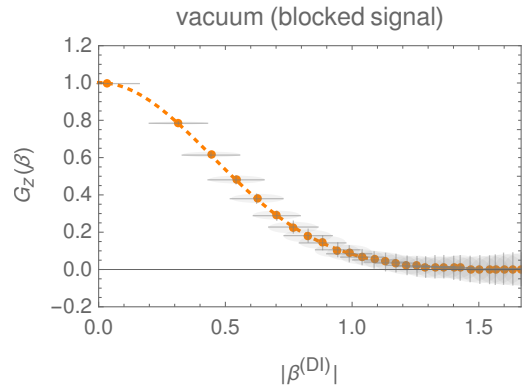


FIG. 8. Phase-space distribution for vacuum, $G_z(\beta) = G_z^{(\text{vac})}(\beta) = G_z^{(0)}(\beta)$, with $z = -1.5$. The dashed line corresponds to a fit function $f_0 \exp[-b|\beta^{(DI)}|^2]$ for real-valued constants f_0 and b .

of Eq. (B4) with derivatives of delta distributions results in $\left. \partial_{\alpha}^j \partial_{\alpha^*}^j f(\beta - t\alpha/r) \right|_{\alpha=0} = (-t/r)^j (-t^*/r^*)^j \partial_{\beta}^j \partial_{\beta^*}^j f(\beta)$.

From Eq. (H1) and the fit obtained from $G_z^{(0)}(\beta)$, we can therefore predict the phase-space distribution of an m -photon state. In our case, this means that $G_z^{(m)}(\beta)$ is a Gaussian function multiplied with a fixed m th-order polynomial in $|\beta|^2$. In this context, also recall the linear relation between the actual intensity (via the setting number n) and the detector-independent intensity in Fig. 4. In addition, it is known (see, e.g., Ref. [83]) that imperfect heralding for the kind of photon source used leads to additional noise contributions. For this reason, our fit for an heralding to the k_h th bin is described through $G_z^{(k_h)}(\beta) = \sum_{j=0}^{k_h} f_j |\beta^{(\text{DI})}|^{2j} \exp[-b|\beta^{(\text{DI})}|^2]$, which constitutes the generalized fit function used in the main text [Figs. 2(a)–(c)] and is determined from the vacuum measurements alone and without relying on any detection models.

As a final remark, it is worth mentioning that the above treatment can be straightforwardly generalized to predict $G_z(\beta)$ for arbitrary states, resulting in Eq. (8) in the main text. This is based on the fact that the P function of an arbitrary state can be written as a convolution, $P(\alpha) = \int d^2\alpha' P(\alpha - \alpha') P^{(0)}(\alpha')$, recalling that the vacuum state is described by a delta distribution, $P^{(0)}$. Thus, Eq. (B4) implies that G_z of an arbitrary state, represented through the Glauber-Sudarshan distribution P , is predicted to resemble the convolution of the already measured vacuum state's $G_z^{(0)}$ and P . Even more generally, we can write

$$g_{z_0, \dots, z_K}(\beta) = \int d^2\alpha P(\alpha) g_{z_0, \dots, z_K}^{(0)}\left(\beta - \frac{t}{r}\alpha\right), \quad (\text{H2})$$

where $g_{z_0, \dots, z_K}^{(0)}(\beta) = [\sum_{k=0}^K z_k P_k(-r\beta/\sqrt{N})]^N$, cf. Eq. (B3), to predict the phase-space distribution for a state, theoretically described through $P(\alpha)$, via the measured $g_{z_0, \dots, z_K}^{(0)}$.